



Comparison of ultraviolet spectroradiometers in Antarctica

Germar Bernhard,¹ Richard L. McKenzie,² Michael Kotkamp,² Stephen Wood,² Charles R. Booth,¹ James C. Ehamjian,¹ Paul Johnston,² and Sylvia E. Nichol³

Received 10 October 2007; revised 30 January 2008; accepted 14 March 2008; published 26 July 2008.

[1] Solar ultraviolet irradiance has been monitored in Antarctica for almost two decades by a network of spectroradiometers established by the National Science Foundation. Data have been used for investigating increases in ultraviolet radiation in response to ozone depletion, validation of satellite observations, and the establishment of ultraviolet radiation climatologies and trends. To assess the quality of data collected, measurements of the monitoring spectroradiometer installed at Arrival Heights (78°S, 167°E) were compared with an independently calibrated, state-of-the-art instrument, which was installed next to the monitoring system for a three-month campaign. Measurements of the two instruments differed by 5–7% on average. The discrepancy is quantitatively explained by the different irradiance scales used by the two systems, a bias in determining the reference plane of fore-optics, drifts of calibration standards, some temperature-dependence in the transmission of the entrance optics, and nonlinearity of one of the systems. The wavelength accuracy of data from both instruments was also tested with two commonly used correlation methods. Wavelength shifts determined with the two methods agreed to within 0.003–0.006 nm. Results of the campaign suggest that data collected by the monitoring instrument are of adequate quality for submission to the Network for the Detection of Atmospheric Composition Change.

Citation: Bernhard, G., R. L. McKenzie, M. Kotkamp, S. Wood, C. R. Booth, J. C. Ehamjian, P. Johnston, and S. E. Nichol (2008), Comparison of ultraviolet spectroradiometers in Antarctica, *J. Geophys. Res.*, 113, D14310, doi:10.1029/2007JD009489.

1. Introduction

[2] The U.S. National Science Foundation's (NSF) Ultraviolet Spectral Irradiance Monitoring Network (UVSIMN) was established in 1987 for measuring ultraviolet (UV) radiation at high latitudes [Booth *et al.*, 1994]. The network primarily employs SUV-100 spectroradiometers, is operated by Biospherical Instruments Inc (BSI), and currently includes seven sites, three of which are in Antarctica. Network data have been used for studies investigating increases in UV in response to ozone depletion [Booth and Madronich, 1994]; research into factors affecting UV irradiance at the Earth's surface [e.g., Zerefos *et al.*, 2001; Nichol *et al.*, 2003; Bernhard *et al.*, 2007]; validation of satellite UV observations [Kalliskota *et al.*, 2000; Tanskanen *et al.*, 2007]; validation of radiative transfer model calculations [e.g., Kancler *et al.*, 2005; Bernhard *et al.*, 2007]; and the establishment of UV climatologies and trends [Bernhard *et al.*, 2004, 2006b, 2007]. Data have further been used by biologists analyzing the effects of UV irradiance on aquatic [e.g., Smith *et al.*, 1992] and terrestrial [Day *et al.*, 1999] ecosystems. Data accuracy is of crucial

importance for most of these applications. The objective of this paper is to quality-assure UVSIMN measurements against data from an independently calibrated and maintained state-of-the-art instrument, which is part of the Network for the Detection of Atmospheric Composition Change (NDACC).

[3] Quality control of network data [Bernhard *et al.*, 2006a] and the correction of known systematic errors [Bernhard *et al.*, 2004, 2006b] has high priority. Network instruments have successfully participated in national and international intercomparisons [Seckmeyer *et al.*, 1995; Thompson *et al.*, 1997; Early *et al.*, 1998; Lantz *et al.*, 2002; Wuttke *et al.*, 2006a]. For example, measurements of erythemal irradiance performed by an SUV-100 instrument at an intercomparison in 1994 agreed to within 7% with results from four other instruments from Germany, New Zealand, and Australia [Seckmeyer *et al.*, 1995]. This intercomparison formed the basis for a study on geographical differences in UV radiation featuring twelve sites from both hemispheres. For wavelengths larger than 315 nm, measurements of an SUV-150B spectroradiometer (an advanced version of the SUV-100) operated by BSI at an intercomparison in 2003 agreed to within $\pm 5\%$ with measurements performed by the University of Hannover, Germany, and New Zealand's National Institute of Water and Atmospheric Research (NIWA) [Wuttke *et al.*, 2006a]. The NIWA instrument was largely identical to the UV9 spectroradiometer discussed in this paper. Differences in the order of $\pm 5\%$ may seem large but represent the typical level

¹Biospherical Instruments Inc., San Diego, California, USA.

²National Institute of Water and Atmospheric Research (NIWA), Lauder, Central Otago, New Zealand.

³National Institute of Water and Atmospheric Research, Kilbirnie, Wellington, New Zealand.

of discrepancy between solar UV measurements performed by state-of-the-art spectroradiometers [Bais *et al.*, 2001].

[4] While these campaigns were of great value for assessing the systems' performance, there is no final proof that results can be applied to instruments permanently installed in Antarctica. Operating radiometers on this continent presents unique challenges, such as low ambient temperatures (also during calibrations), low humidity, small solar elevations, potentially large changes in collector temperature, high wind speeds, large and highly variable surface albedo, snow accumulation, and 24 h of sunlight during summer. All these factors can affect data quality.

[5] For directly assessing the quality of network instruments operated in Antarctica, an intercomparison was organized between November 2006 and January 2007 at Arrival Heights, Antarctica. The SUV-100 instrument that is permanently installed at this location was compared with a spectroradiometer built and operated by NIWA. The NIWA instrument is part of a larger network, is an established system of NDACC, and instruments of this type have successfully participated in intercomparisons [Bais *et al.*, 2001; Wuttke *et al.*, 2006a]. An additional goal of the campaign was to determine whether SUV-100 data meet the standards of UV spectroradiometry established by NDACC. A positive outcome would encourage submission of UVSIMN data to the NDACC database. In the future, we are also planning to assess geographical differences of UV radiation using data from both networks. Results of the campaign will form a solid foundation for this work.

2. Location

[6] The intercomparison took place at Arrival Heights (77°49'46"S, 166°39'45"E, 183 m above sea level (a.s.l.)) between 12 November 2006 and 12 January 2007. Arrival Heights refers to a hill-top location and is situated approximately 3 km north of McMurdo Station, the largest research and logistics hub in Antarctica. New Zealand's Scott Base is approximately 4 km south–west of Arrival Heights. The area of interest is located on the southern tip of Ross Island and is surrounded by the Ross Sea to the north and the Ross Ice Shelf to the south. The active volcano Mount Erebus (3795 m a.s.l.) is 34 km north of the instrument. Most of Ross Island is covered by snow and ice year-round, however, an area with a radius of approximately 1–2 km around the intercomparison site was snow-free, and dark volcanic rocks were exposed. Weather conditions ranged from clear-sky to overcast, and temperatures varied between –25°C and +5°C in November and –15°C and +8°C in December and January.

3. Instrumentation

3.1. SUV-100 Spectroradiometer

[7] The instrument operated by BSI is a high-resolution SUV-100 spectroradiometer, designed and built by BSI, and installed at Arrival Heights in March of 1988. Instruments of the same type are used at all sites of the NSF UVSIMN, with the exception of Summit, Greenland, where a SUV-150B has been installed. Instruments measure spectra of global solar irradiance between 280 and 600 nm with a spectral resolution of approximately 1.0 nm at a rate of 4

spectra per hour. The instrument has a comparatively large cosine error of –8.5% at 60° and –19% at 75°. Additional specifications are provided in Table 1. The instrument is calibrated every two weeks with 200-Watt standards of spectral irradiance, which are traceable to the 1990 source-based scale of the U.S. National Institute of Standards and Technology (NIST) [Walker *et al.*, 1987]. Measurement and calibration protocols during the intercomparison were the same as implemented during normal operation. SUV-100 spectroradiometers and their calibration have been described in detail by Booth *et al.* [1994] and NSF Network Operations Reports [e.g., Bernhard *et al.*, 2006a]. Measured spectra were corrected for the cosine error of the instrument, aligned against the Fraunhofer structure of a reference solar spectrum (provided at sea level pressure), resampled to a uniform wavelength grid, and normalized to a uniform bandwidth of 1 nm. (Normalized spectra appear as if they were measured with a spectroradiometer that has a triangular slit function of 1.0 nm full width at half maximum (FWHM)). These data processing steps have been described by Bernhard *et al.* [2004, 2006b], and resulting data are known as “Version 2 NSF Network Data.” Additional information is provided at www.biospherical.com/nsf/Version2/. The expanded standard uncertainty of erythemal irradiance (CIE action spectrum by McKinlay and Diffey [1987]) and spectral irradiance at 400 nm varies between 4.2% and 6.8% (coverage factor 2, corresponding to a confidence level of 95.5% or 2 σ -level) [Bernhard *et al.*, 2006b]. Expanded uncertainties at 600 nm are dominated by uncertainties of the cosine error correction, and can be as high as 16% for low-Sun, scattered-cloud conditions.

3.2. UV9 Spectroradiometer

[8] The instrument operated by NIWA is based on a Bentham DTM300 double monochromator and has the designation UV9. In normal operation, global spectral irradiance is measured between 285 and 450 nm in 0.2 nm steps with a spectral resolution of approximately 0.6 nm and at 5° steps in solar zenith angle (SZA). For the purpose of the intercomparison, the measurement protocol was modified to match the sampling scheme of the SUV-100 (section 5). The cosine error of the instrument is smaller than $\pm 3\%$ for SZA up to 70°. A detailed description of the instrument can be found at www.niwasience.co.nz/rc/fac/instruments/lauder/uvspec. Additional information is provided in Table 1 and in the work by Wuttke *et al.* [2006a]. Similar instruments have been permanently installed at Lauder, New Zealand; Mauna Loa Observatory, Hawaii; Boulder, Colorado; Alice Springs, Australia; and Tokyo, Japan. They have also operated for extended periods in Melbourne and Darwin, Australia. This particular instrument has operated in Lauder and Thule, Greenland.

[9] Calibrations are traceable to NIST via 1000-Watt FEL quartz-halogen lamps. Instrument stability is tracked with stabilized 45-Watt quartz-halogen lamps. Measurements with these lamps were performed once per week during the campaign, both in a constant current mode of operation and in a feedback mode to provide a constant signal from a UV-A diode. The transfer of calibrations from 1000-Watt to 45-Watt lamps includes an uncertainty of $\pm 1\%$, which was estimated from the repeatability of scans with the 45-Watt lamp.

Table 1. Comparison of Instrument Specifications

Specification	SUV-100	UV9
Monochromator	ISA DH-10UV; double monochromator; additive dispersion; focal length 100 mm; focal ratio $f/3.5$; equipped with spherical holographic gratings with 1200 lines/mm	Bentham, DTM300; double monochromator; additive dispersion; focal length 300 mm; focal ratio $f/4.2$; equipped with plane holographic gratings with 3600 lines/mm
Operational wavelength range	280–605 nm	285–450 nm
Operational sampling step	0.2 nm between 280 and 345 nm; 0.5 nm between 335 and 405 nm; 1.0 nm between 395 and 605 nm ^a	0.2 nm integrations, with at least 5 samples per integration
Bandwidth (FWHM)	approximately 1.0 nm in UV; 0.8–0.95 nm in visible	0.52–0.58 nm in UV; 0.5 nm in visible
Entrance optics	In-house designed diffuser made of polytetrafluoroethylene (PTFE) covering a trapezoidally shaped quartz support	In-house designed shaped diffuser made of PTFE ^b
Cosine error	–8.5% at 60°, –14% at 70°, –19% at 75°, and –6% to isotropic illumination	±3% for incidence angles <70°; ±1% to isotropic illumination
Coupling	Direct	Quartz fiber
Detector	Photomultiplier R269 from Hamamatsu; bialkali photocathode; thermoelectrically cooled	Photomultiplier R1527 from Hamamatsu
Dynamic range	6 orders of magnitude, achieved by adjusting PMT high-voltage; limited by digitization scheme	7.5 orders of magnitude, achieved with a 24 bit Delta Sigma A to D. Constant PMT high-voltage

^aFor overlapping intervals, data from the segment with the smaller wavelength step increment were used.

^bSee: <http://www.niwascience.co.nz/rc/fac/instruments/lauder/ptfe>.

[10] Standard analysis includes corrections for stray light, dark current, nonlinearities in the wavelength drive using a Fraunhofer-line correlation algorithm [McKenzie *et al.*, 1992], and departures from the ideal angular response. For the purpose of this campaign, spectra were normalized to a bandwidth of 1 nm FWHM with the NSF Version 2 algorithm [Bernhard *et al.*, 2004], and resampled to match the wavelength grid of the SUV-100 instrument.

[11] NIWA instruments meet the NDACC standards [McKenzie *et al.*, 1997; Wuttke *et al.*, 2006a] and specifications of type S-2 instruments as classified by the World Meteorological Organisation (WMO) [Seckmeyer *et al.*, 2001]. Previous measurement intercomparisons [Bais *et al.*, 2001] and comparisons with clear sky models [Badosa *et al.*, 2007] give confidence that the absolute irradiances measured by these systems are generally better than $\pm 5\%$ ($\pm 2\sigma$).

4. Model Calculations

[12] Measurements of the two instruments were also compared with calculations of the radiative transfer model UVSPEC/libRadtran Version 1.01 [Mayer and Kylling, 2005]. These calculations provide a semi-independent data set for comparison, and also help correcting small differences in the timing of the two instruments (section 5). Both instruments are scanning spectroradiometers requiring several minutes for the completion of a spectrum. Model calculations take the change of SZA during the recording of a spectrum into account. Modeled spectra were convolved with a triangular function of 1.0 nm FWHM for comparison with the measurements.

[13] Model inputs for the extraterrestrial spectrum, aerosol extinction, as well as profiles of air density, ozone and temperature were identical to those used by Bernhard *et al.* [2006b]. The model's pseudospherical disort radiative transfer solver with six streams was used. Surface pressure was adopted from hourly measurements at Arrival Heights.

Effective surface albedo [Lenoble *et al.*, 2004] was calculated from spectra measured by the SUV-100 as described by Bernhard *et al.* [2006b] by evaluating the relative enhancement of irradiance at 330 nm compared to irradiance at 400 nm. Errors in the measurement that affect all wavelengths equally do not introduce an error in the calculation of albedo. Nevertheless, when comparing measured and modeled spectra, it has to be taken into account that model calculations are not completely independent of the measurements. Calculated effective albedo was 0.82 ± 0.02 for the second half of November, 0.81 ± 0.02 for December, and 0.77 ± 0.03 for the first half of January. These value agree well with data from this site reported earlier [Bernhard *et al.*, 2006b]. Values are smaller than albedo of fresh snow [Wuttke *et al.*, 2006b] due to snow-free areas around the measurement site.

[14] Total ozone column used for modeling was calculated from SUV-100 spectra using the method described by Bernhard *et al.* [2003]. The algorithm takes cloud attenuation into account. Three ozone values per day (at 01:00, 04:00, and 22:00 UT) were typically determined. Retrievals were intercompared with concurrent measurements of a Dobson spectrophotometer located at Arrival Heights and observations of the Ozone Monitoring Instrument (OMI) onboard the NASA EOS Aura spacecraft. SUV-100 data were also compared with total ozone from UV9 data that were calculated using the method by Bernhard *et al.* [2003] as well as an adaptation of the algorithm described by Stamnes *et al.* [1991]. The latter algorithm is normally used by NIWA. Results of the comparison are shown in Figure 1. For the period of the campaign, the ratio of Dobson to SUV-100 total ozone was 0.976 ± 0.021 ($\pm 1\sigma$). This value is about 1.5% smaller than historic measurements: for data collected between 1989 and 2006, the ratio was 0.990 ± 0.038 . Preliminary analysis indicates that a step-change in Dobson measurements after January 2004 is likely responsible for the difference. The ratio of OMI to SUV-100 was 0.965 ± 0.032 for the period of the campaign. This value

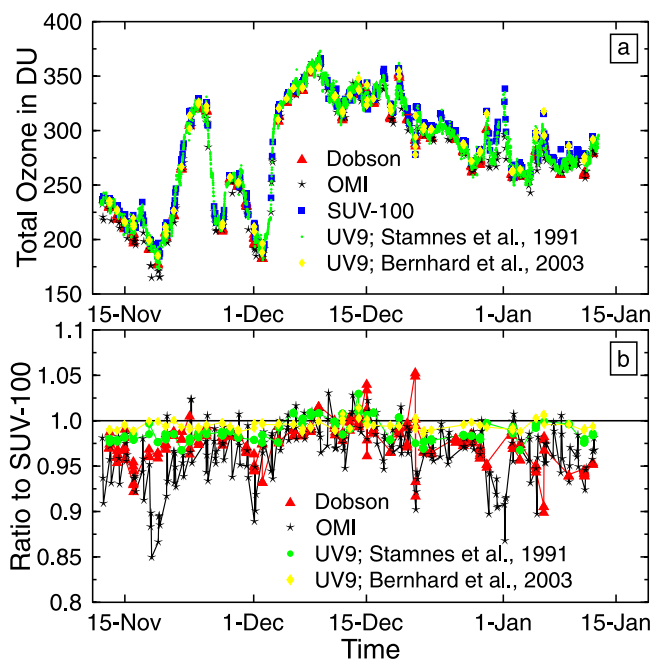


Figure 1. Comparison of total ozone measured by SUV-100, UV9, Dobson, and OMI. UV spectra of the UV9 were processed with the methods by *Stamnes et al.* [1991] and *Bernhard et al.* [2003]. (a) Time series of total ozone data. (b) Ratio of total ozone measurements relative to SUV-100 data.

compares well with the ratio of 0.969 ± 0.044 between Earth Probe TOMS and SUV-100 measurements from the period 1996–2004 reported by *Bernhard et al.* [2006b]. The reason for the $\sim 3.5\%$ bias between SUV-100 and space-based measurements at this site is currently unknown. We note that this bias is larger than typical differences between OMI and ground-based total ozone observations reported by *Balis et al.* [2007]. The bias (OMI lower) was particularly large on 18 November, 1 December, and 31 December 2006. All 3 days were affected by clouds. Absorption by tropospheric ozone can be increased by clouds due to path length enhancement [*Mayer et al.*, 1998]. Ground-based measurements were likely biased high on these days due to this effect. The ratio of UV9 to SUV-100 was 0.988 ± 0.012 using the algorithm by *Stamnes et al.* [1991] and 0.995 ± 0.005 using the method by *Bernhard et al.* [2003]. The difference is likely caused by the different ozone and temperature profiles used by the two implementations.

5. Intercomparison Protocol and Data Analysis

[15] The intercomparison of the two instruments was “blind;” no calibration or solar data were exchanged before the end of the campaign. Clear-sky spectra were selected from the data set based on temporal variability of spectral irradiance at 600 nm using a similar method as described by *Bernhard et al.* [2004]. Since the method does not depend on absolute irradiance, it is insensitive to potential calibration errors or the cosine error of the instrument’s irradiance collector.

5.1. Synchronization

[16] Measurements of the two instruments were synchronized between 285 and 340 nm. Synchronization at longer wavelengths was not possible due to the fact that the SUV-100 measures a spectrum in three different, overlapping segments (Table 1). Different PMT high-voltage and wavelength increments are applied in each of the segments to optimize signal-to-noise ratio and scan duration [*Bernhard et al.*, 2006a]. Figure 2 shows the relationship between time and wavelength for the two instruments. From 340 nm to 450 nm, the UV9 spectroradiometer measured faster than the SUV-100. Because of this time difference, measurements in the visible by UV9 are expected to be smaller in the morning and larger in the afternoon than corresponding measurements by the SUV-100. Comparison of measured spectra confirmed this. To correct for this artifact, we consider the ratio $R(\lambda, t)$ when comparing the two instruments:

$$R(\lambda, t) = \frac{M_{SUV}(\lambda, t)/C(\lambda, t)}{M_{UV9}(\lambda, t^*)/C(\lambda, t^*)},$$

where $M_{SUV}(\lambda, t)$ is spectral irradiance measured by the SUV-100 at wavelength λ and time t , $M_{UV9}(\lambda, t^*)$ is spectral irradiance measured by the UV9 at wavelength λ and time t^* , and $C(\lambda, t)$ and $C(\lambda, t^*)$ are the corresponding model irradiances at time t and t^* . For wavelengths below 340 nm, t equals t^* and $R(\lambda, t)$ defaults to $M_{SUV}(\lambda, t)/M_{UV9}(\lambda, t)$.

5.2. Analysis of Wavelength Accuracy

[17] The wavelength accuracy of SUV-100 and UV9 measurements was assessed with the Fraunhofer-line correlation algorithm of the NSF Version 2 data processing suite [*Bernhard et al.*, 2004] and a similar algorithm that is part of the SHICrvm software package, available at www.rivm.nl/shicrvm [*Slaper et al.*, 1995]. The wavelength reference of both algorithms is based on the “Kitt Peak solar flux atlas” [*Kurucz et al.*, 1984]. This spectrum was measured with a high-resolution (approximately 0.0001 nm) Fourier Transform Spectroradiometer and refers to mean sea surface pressure of 1013 hPa. Its wavelength accuracy was confirmed to be better than 0.001 nm by comparing the position of its Fraunhofer-lines with the wavelengths of tabulated electronic transitions [*Bernhard et al.*, 2004].

[18] The two algorithms use different methods for correcting small errors in the radiometric calibration of the Kitt Peak spectrum, which are most prominent between 320 and

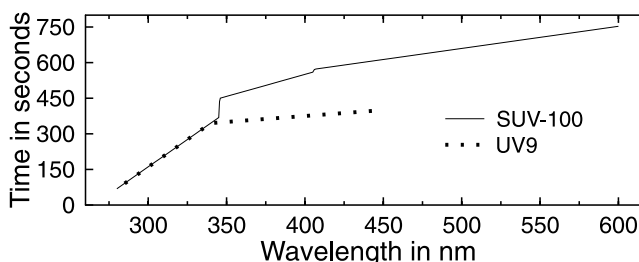


Figure 2. Relationship between time and wavelength for the SUV-100 and UV9 instruments.

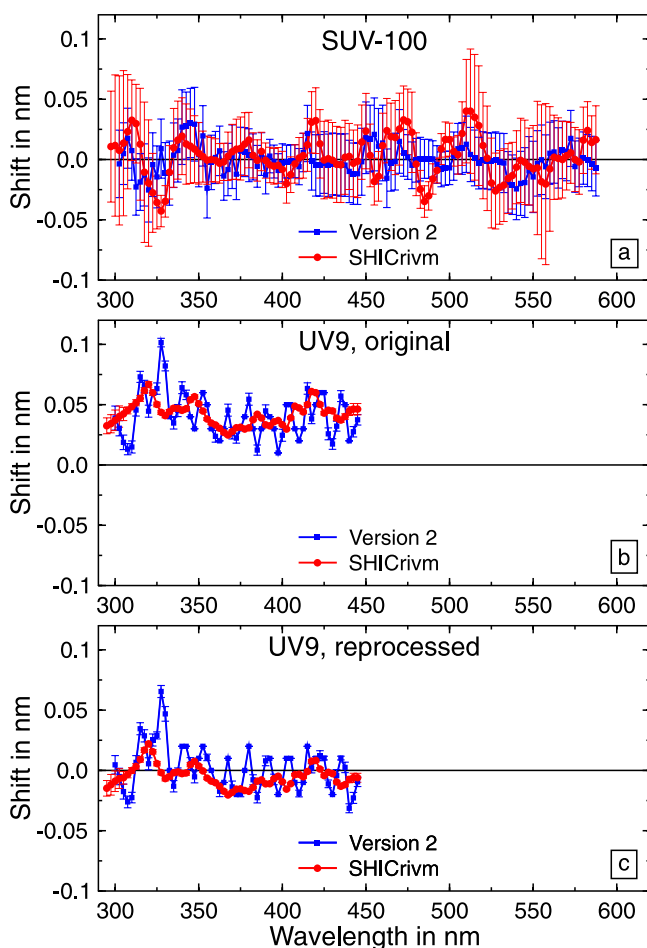


Figure 3. Wavelength accuracy of data from the SUV-100 and UV9 instruments determined with the Version 2 and SHICrvm methods. Symbols indicate average shifts calculated from all spectra measured during the campaign. Error bars indicate the standard deviation of shifts. (a) SUV-100. (b) Original data of UV9. (c) Reprocessed data of UV9.

330 nm. The correction for the Version 2 algorithm (hereinafter referred to as V2 method) is based on the extraterrestrial spectrum proposed by Gueymard [2004]. The resulting reference spectrum is identical with the spectrum “ $E_{\text{Gueymard}}(\lambda)$ ” introduced by Bernhard *et al.* [2004]. The reference spectrum of the SHICrvm method has been described by Slaper and Koskela [1997].

[19] Besides distinctions in the reference spectra, the two correlation methods differ also in several other ways: the V2 method allows for adjustment of the spectroradiometer’s slit function as a function of wavelength. This feature is of value for the SUV-100, whose bandwidth changes from 1.05 nm FWHM at 300 nm to 0.80 nm at 600 nm. In contrast, the bandwidth of the SHICrvm algorithm is fixed for all wavelengths. When using SHICrvm, we chose triangular slit functions with 1.0 and 0.6 nm FWHM for the SUV-100 and UV9 instrument, respectively. The correlation interval can be specified in both methods. For processing data of the UV9 instrument with the V2 method, the interval was set to ± 3 nm at all wavelengths. For the

SUV-100, it was set to ± 3 nm in the UV and ± 15 nm in the visible. The larger interval in the visible is necessary since SUV-100 data are not oversampled between 404 and 600 nm (Table 1). For SHICrvm processing, the interval was set to the default setting of ± 8 nm at all wavelengths for both instruments. This resolution was chosen because preliminary runs with a finer resolution led to sporadic spikes in the results.

6. Results

6.1. Wavelength Accuracy

[20] Figure 3 shows the wavelength accuracy of data from the SUV-100 and UV9 instruments as determined with the V2 and SHICrvm programs. Additional statistics are provided in Table 2. The average shift for the SUV-100 data set is smaller than ± 0.003 nm for both algorithms (Figure 3a). This good agreement was expected as the V2 method was used for the preparation of SUV-100 data. The standard deviation of the shifts (illustrated by errors bars in Figure 3a), is about 0.025 nm, indicating some variations in the wavelength calibration during the period of the campaign.

[21] The wavelength alignment of data from the UV9 instrument was based on the ATLAS-3 solar spectrum [van Hoosier, 1996] as implemented by the TUV radiative transfer model [Madronich and Flocke, 1998]. However, a subsequent wavelength shift of 0.04 nm had also been applied so that the shift matched that from an earlier software version for data processing, which had been based on a filtered version of the Lowtran spectrum [Kneizys *et al.*, 1983]. Analysis of UV9 spectra with the V2 and SHICrvm programs revealed a systematic wavelength shift of 0.04 nm (Figure 3b). This suggests that the absolute wavelength scale of ATLAS-3 scale was more correct. We further discovered that there is a 0.04 nm error in the Lowtran spectrum in the region of the Ca Fraunhofer doublet near 390 nm, which has a strong influence on the wavelength alignment for the NIWA instruments.

[22] To ensure compatibility with the model calculations, UV9 data was reprocessed by NIWA using the $E_{\text{Gueymard}}(\lambda)$ reference spectrum, which had also been implemented for SUV-100 data. Analysis of the reprocessed version indicates that the wavelength bias of 0.04 nm was successfully removed; the residual shift is 0.005 nm on average (Figure 3c). The change in wavelength alignment also reduced the measurement bias between the two systems in the UV-B. For example, erythral irradiance calculated from the reprocessed data set is 0.5% smaller and in better agreement with SUV-100 data. In the UV-A, the effect may be neglected. For the remainder of this paper, the discussion

Table 2. Statistics of Wavelength Shift

Data set	Method	Average Bias ^a , nm	Average Variability ^b , nm
SUV-100	Version 2	−0.001	0.023
SUV-100	SHICrvm	0.003	0.029
UV9, original	Version 2	0.040	0.003
UV9, original	SHICrvm	0.043	0.002
UV9, reprocessed	Version 2	0.001	0.003
UV9, reprocessed	SHICrvm	−0.005	0.002

^aAverage wavelength shift of all data points of Figure 2.

^bAverage standard deviation for all data points of Figure 2.

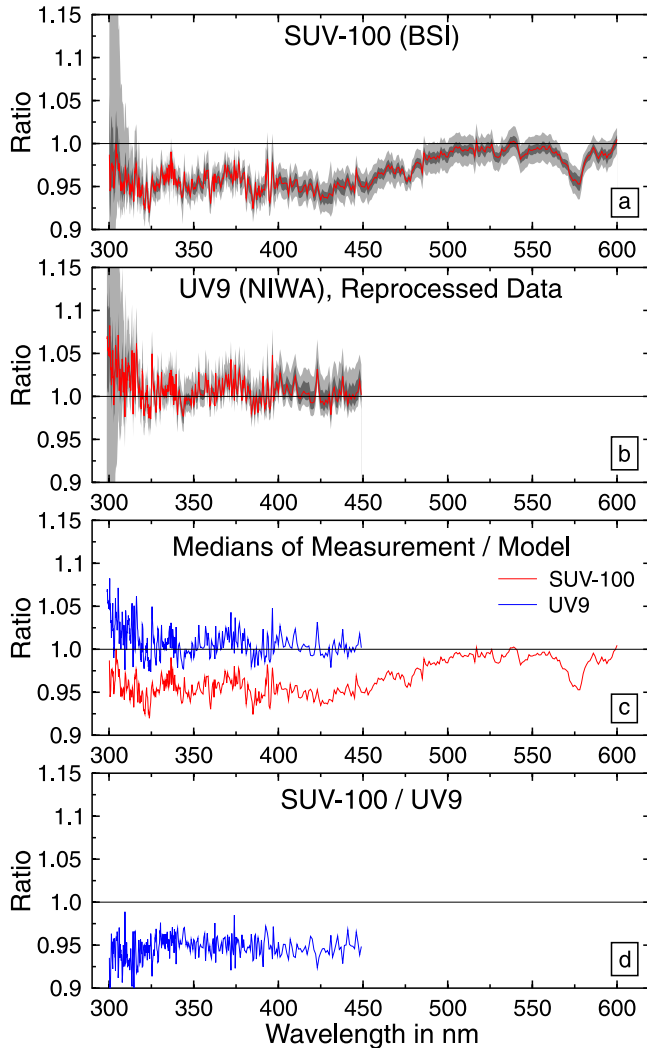


Figure 4. Comparison of spectra measured by the SUV-100 and UV9 instruments during clear skies with calculations of the radiative transfer model. (a) Ratio of SUV-100 to model. Solid line is the median of all 1197 clear-sky spectra measured during the campaign. Dark gray shading indicates the 50th percentile, and light gray shading the 90th percentile of ratio-spectra. (b) Ratio of the reprocessed UV9 data set to the model. (c) Median ratio-spectra for the two data sets. (d) Ratio of median ratio-spectra from Figure 4c.

of NIWA data will focus on this reprocessed data set. The wavelength shift variability of UV9 data is about ± 0.0025 nm ($\pm 1\sigma$). This exceptionally low value is a factor of 10 smaller than the uncertainty of the SUV-100 data set.

[23] Data from both spectroradiometers indicate that wavelength shifts of the V2 and SHICrvm algorithms are on average consistent at the 0.003–0.006 nm level (Table 2). Some discrepancies of the two algorithms can be explained by the different correlation intervals used. For example, wavelength shifts calculated for the UV9 instrument with the V2 method reveal oscillations on a 10 nm scale. These fluctuations are not apparent in the SHICrvm data set presumably due to its coarser resolution. When using the V2 method for analyzing spectra of the SUV-150B spectroradiometer installed at Summit (which has a similar

bandwidth as the UV9), we did not observe oscillations similar to those shown in Figures 3b and 3c [Bernhard *et al.*, 2006a]. At this stage, we do not know whether these oscillations are real or an artifact of the V2 program when applied to UV9 spectra.

6.2. Comparison of Spectral Irradiance

[24] Spectra measured by the two instrument at SZAs smaller than 80° during clear-skies were selected from the data set and ratioed against the complementing model spectra. The total number of ratio-spectra was 1197 for the SUV-100 and 1133 for the UV9. Medians of these ratio-spectra were calculated on a wavelength by wavelength basis and are shown as red lines in Figures 4a and 4b. Dark gray shading indicate the 50th percentile, and light gray shading the 90th percentile of the ratio-spectra.

[25] For the SUV-100, the median ratio-spectrum is about 0.96 in the UV-B (here defined as 300–315 nm), 0.955 in the UV-A, and between 0.95 and 1.00 in the visible (Figure 4a). Drops in the ratio near 477 and 577 are caused by absorption of the O_2 – O_2 collision complex [Greenblatt *et al.*, 1990], which is not considered by the model. The distribution of ratio-spectra about the median is very narrow: in the UV-A and visible, 50% (90%) of the spectra fall within a range of $\pm 1\%$ ($\pm 2.5\%$). A somewhat larger spread is observed in the UV-B. This is mostly caused by changes in total ozone, which is not always tracked with sufficient temporal resolution by the model.

[26] For the UV9 data, the median ratio is about 1.026 in the UV-B, 1.005 in the UV-A, and 1.003 in the visible (Figure 4b). 50% (90%) of the spectra fall within a range of $\pm 1\%$ ($\pm 2.5\%$). These percentages are virtually identical to those for the SUV-100.

[27] The median ratio-spectra of the two data sets are also plotted in Figure 4c. Ratios of the SUV-100 and UV9 show similar patterns on a 10–20 nm scale. For example, there are local maxima at 335, 375, and 395 nm in all data sets. These common patterns are mostly caused by the model, specifically the extraterrestrial spectrum. Similar patterns have also been observed at other network sites of the NSF UVSIMN, and have been discussed by Bernhard *et al.* [2004].

[28] Figure 4c may suggest that UV9 measurements are in better agreement with the true spectral irradiance than SUV-100 data. However, data of both instruments are referenced to the model, which is also subject to error. For example, a similar wavelength dependence than that shown in Figures 4a and 4c would be expected if SUV-100 measurements had been correct and the effective albedo used for modeling had been too high. If albedo in the model had been reduced by 0.1 (which is about the uncertainty of the albedo estimate), SUV-100 measurements would have been in good agreement with the model.

[29] Figure 4d shows the ratio $R(\lambda, t)$ of SUV-100 to UV9 based on the median ratio-spectra of Figure 4c. By forming this double-ratio, the influence of the model is removed, except for the small effect from the synchronization correction discussed in section 5.1. The ratio is about 0.94 in the UV-B, and 0.95 in the visible.

[30] In Figure 5, we plotted the synchronization-corrected ratios $R(\lambda, t)$ of SUV-100 / UV9 as a function of SZA for several wavelengths. The clear-sky subset is indicated by

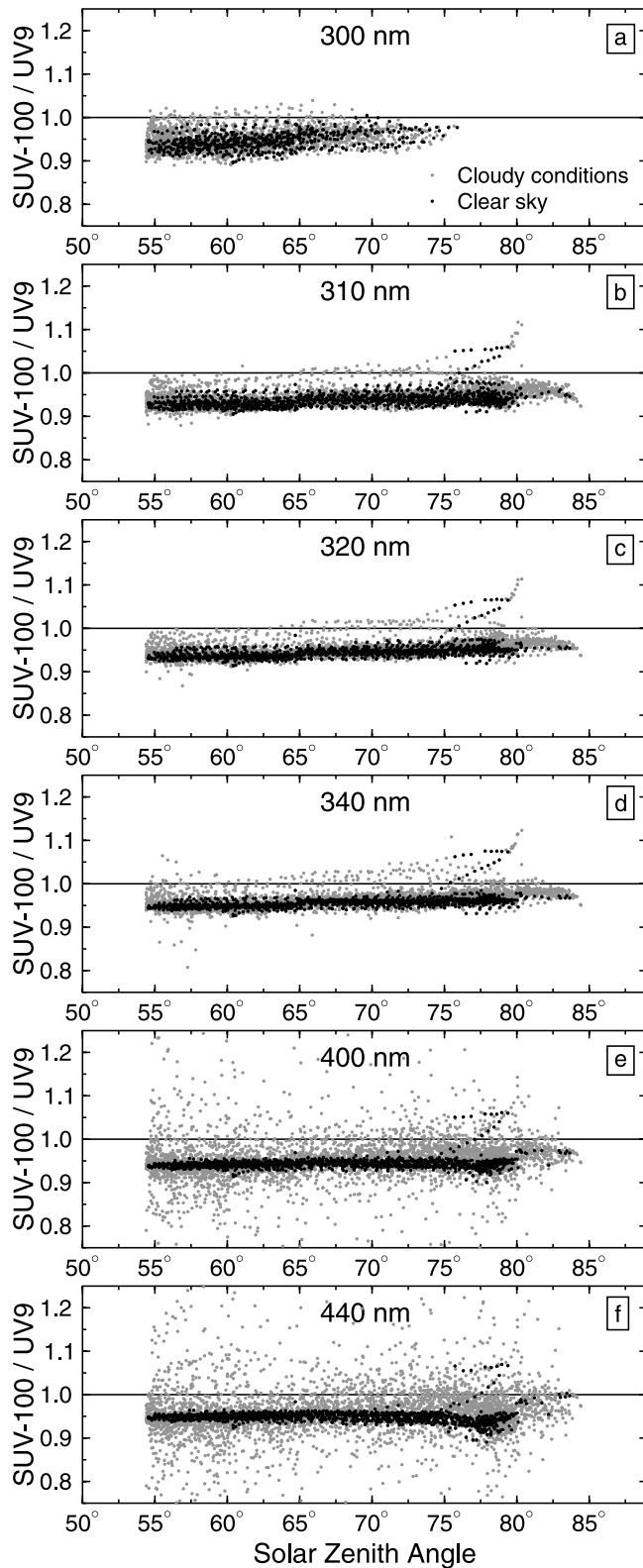


Figure 5. Synchronization-corrected ratios of SUV-100 to UV9 as a function of SZA for several wavelengths. Black (gray) dots indicate clear sky (cloudy sky) conditions. (a) 300 nm, (b) 310 nm, (c) 320 nm, (d) 340 nm, (e) 400 nm, and (f) 440 nm.

black dots; data collected during partly cloudy or overcast conditions are marked with gray dots. When the SZA is larger than 75° , spectral irradiance at 300 nm is typically below the detection limit of the SUV-100, limiting the SZA-range of Figure 5a. For wavelengths below 340 nm, the SZA-dependence is virtually identical for clear and cloudy situations (Figures 5a–5d). With the exception of a few outliers (which can be explained by collector contamination due to snow or shading by the operator), ratios are very compact and typically fall within a range of $\pm 2.5\%$. The small number of outliers is attributable to the good (± 5 s) synchronization of the two instruments in this wavelength range. Close inspection of Figures 5a–5d reveals steps on the order of 0.5%–1.5% at SZAs of 65° , 75° , and 80° . These steps coincide with the change of high-voltage applied to the PMT of the SUV-100 instrument and indicate some nonlinearity in SUV-100 measurements.

[31] At 400 and 440 nm (Figures 5e and 5f), scatter remains small for the clear-sky subset due to the synchronization correction. However, this correction only reduces the effect of differences in SZA, but cannot correct for changes in irradiance due to moving clouds. The scatter at 400 and 440 nm for the cloudy-sky subset is therefore much larger than for the smaller wavelengths. Despite the difference in scatter, the average biases of the clear-sky and cloudy-sky subsets are similar: at 440 nm and SZAs less than 60° , $R(\lambda, t)$ is 0.95 on average for both subsets. For $60^\circ < \text{SZA} < 70^\circ$, $R(\lambda, t)$ is 0.95 for the clear-sky and 0.96 for the cloudy-sky data; for $70^\circ < \text{SZA} < 80^\circ$, $R(\lambda, t)$ is 0.94 for the clear-skies and 0.96 for cloudy-skies. The differences between the two subsets are within the uncertainties of the V2 cosine error correction [Bernhard *et al.*, 2006b], indicating that the algorithm is treating both sky conditions appropriately.

[32] In Figure 6, $R(\lambda, t)$ -ratios at 440 nm are plotted as a function of solar azimuth angle to examine whether the bias between SUV-100 and UV9 measurements is different in the morning and afternoon. In the morning, the Sun moves from an azimuth angle of 180° to 0° ; in the afternoon, it moves from 360° to 180° . This figure indicates that there is very little difference between morning and afternoon.

[33] Measured spectra were also weighted with the action spectra for erythema [McKinlay and Diffey, 1987], DNA-damage [Setlow, 1974], generalized plant response [Caldwell, 1971], and Vitamin D production [Bouillon *et al.*, 2006]. Ratios of SUV-100 to UV9 are virtually identical to those for spectral irradiance at 310 nm, plotted in Figure 5b. For SZAs smaller than 80° , the average ratio of SUV-100 and UV9 is between 0.948 and 0.955 for all four data products.

[34] In Figure 7, various quantities measured between 6 December and 12 December 2006 are plotted versus time to investigate the effect of clouds on UV and ozone measurements in more detail. The period is divided into four subperiods with different cloud conditions, labeled A, B, C, and D on top of Figure 7. Period A is the clear-sky case. For the UV9, the ratio of measured and modeled spectral irradiance at 440 nm (Figure 7d) is close to 1, but exhibits two small ($<4\%$) bumps at either side of measurements with the largest SZA, which are indicative of an incomplete correction of the instrument's cosine error. Measurements of the SUV-100 show somewhat less vari-

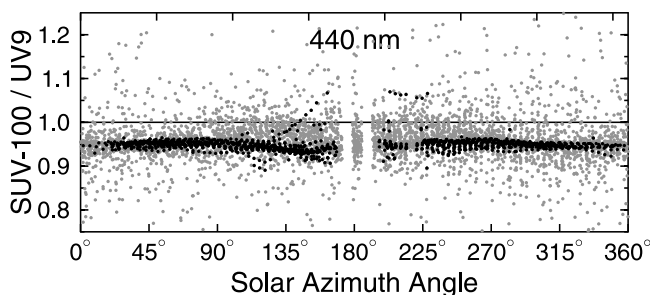


Figure 6. Synchronization-corrected ratios of SUV-100 to UV9 as a function of solar azimuth angle at 440 nm. Black (gray) dots indicate clear sky (cloudy sky) conditions.

ability but are biased low against the model by 4–7%. Ozone measurements of the UV9 are based on the method by *Stamnes et al.* [1991] and show a larger dependence on SZA for $SZA > \sim 70^\circ$ than SUV-100 data, presumably due to the consideration of the actual ozone profile in the method by *Bernhard et al.* [2003] used for the SUV-100 data set (Figure 7f). In Period B, thin and variable clouds were prevailing. $R(\lambda, t)$ -ratios at 310 and 440 nm increase by about 7% from the start to the center of the period and decrease by the same amount thereafter (Figure 7e). This pattern does not correlate with cloud cover and the most likely reason is snow covering the UV9 collector, which is not heated. Persistent cloud cover with an optical depth of approximately 35 (Figure 7c) was observed in Period C. The ratio of measurement and model dropped to 0.5 for both instruments. $R(\lambda, t)$ -ratios for Periods A and C are very consistent, confirming that the cosine error correction of the SUV-100 works well for clear and cloudy conditions. Ozone measurements of both instruments do not change at the end of Period C when cloud optical depth decreased to zero, indicating that the effect of clouds on ozone retrievals is small. Period D is again a period of variable cloudiness when noon-time measurements are reduced by about 20%. $R(\lambda, t)$ -ratios at 440 nm (but not 310 nm) exhibit considerably scatter. Unlike the earlier periods, the scatter seems to be larger for SUV-100 than UV9 data, but the average bias is similar to that of Period A.

6.3. Detection Limit

[35] The V2 and SHICrvm programs both include routines to determine the minimum wavelength from which onward spectra can be trusted. The routines first calculate the ratio of measurement and model as a function of wavelength. The minimum wavelength is defined as the wavelength for which ratios of five consecutive wavelength pairs deviate by less than 25% from each other. The spectral irradiance associated with the minimum wavelength defines the detection limit. Note that this definition of the detection limit is different from that in the NDACC specifications [*McKenzie et al.*, 1997] discussed further below.

[36] Figure 8 shows the minimum wavelength and the associated spectral irradiance for both instruments as a function of time. For the SUV-100, the minimum wavelength varies between 293 and 302 nm. It is largest during solar noon (approximately 01:00 UT), when the SZA is smallest, and smallest at 13:00 UT when the SZA is largest.

Additional variation is introduced by the total ozone column. On 1 December 2006, when total ozone was 185 DU, the minimum wavelength at noon was 293 nm. On 5 December 2006, when total ozone was 328 DU, it increased to 301.5 nm. The minimum wavelength for the UV9 has a similar pattern, but is shifted downward by about 2.5 nm and covers the range 290–299.5 nm. Figure 8 also shows several data points below 290 nm, which are artifacts.

[37] For the SUV-100, the spectral irradiance associated with the minimum wavelength is between $0.001 \mu\text{W}/(\text{cm}^2 \text{ nm})$ for large SZA and $0.01 \mu\text{W}/(\text{cm}^2 \text{ nm})$ for small SZA.

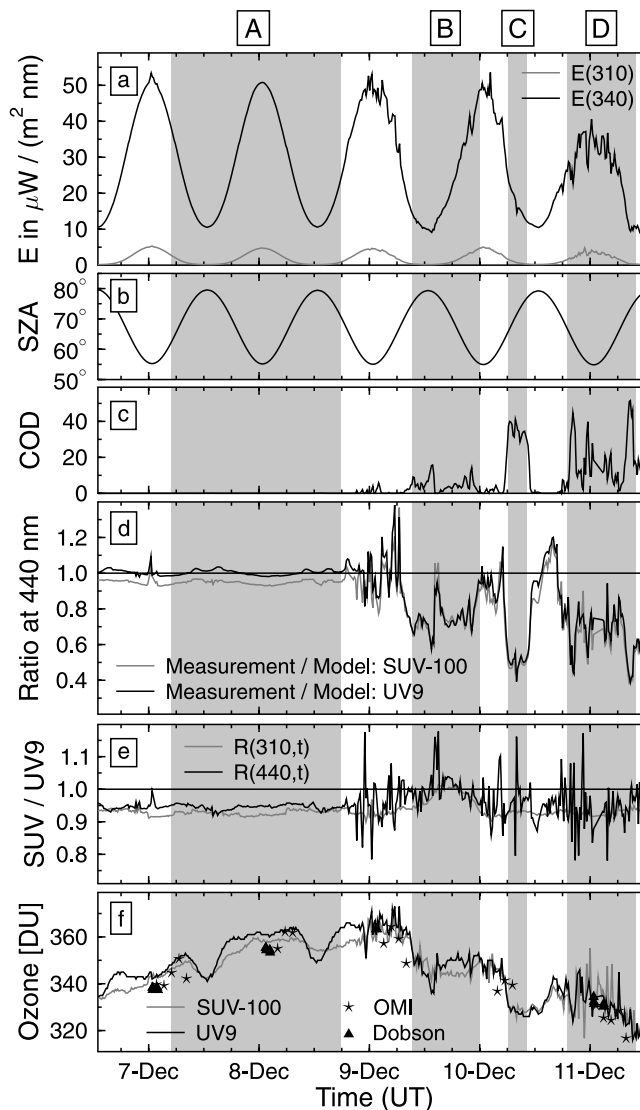


Figure 7. Time series of various quantities measured between 6-December and 12-December 2006. Four periods are emphasized by gray-shading and labeled A, B, C, and D. (a) Spectral irradiance at 310 and 340 nm measured by SUV-100. (b) Solar zenith angle, (c) cloud optical depth (COD), determined from SUV-100 measurements at 450 nm based on the method by *Bernhard et al.* [2004]. (d) Ratio of measurement to model at 440 nm. (e) $R(\lambda, t)$ -ratios (SUV-100 / UV9) at 310 and 440 nm. (f) Total ozone measured by SUV-100, UV9, OMI, and Dobson.

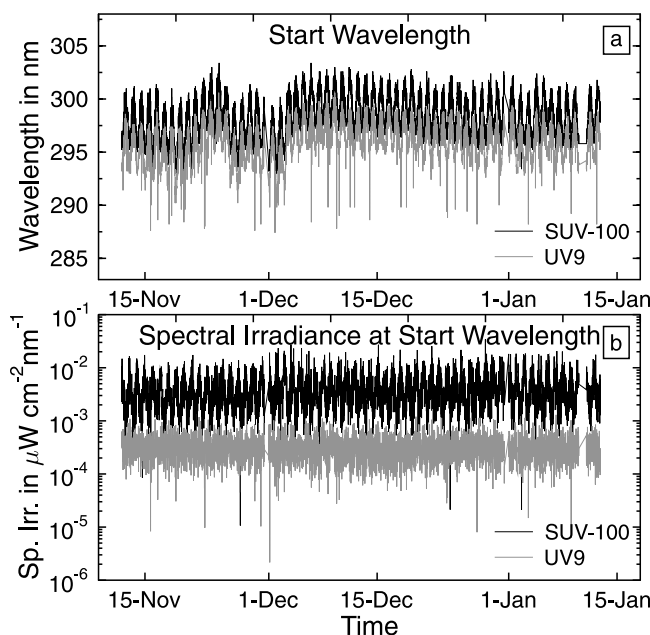


Figure 8. (a) Start wavelength from which onward spectra can be trusted. SUV-100 (UV9) measurements are highlighted by black (gray) lines. (b) Spectral irradiance at start wavelength.

At large SZA, a large high-voltage is applied to the PMT, leading to a better detection limit. The high-voltage is reduced at small SZAs to avoid saturation of the PMT. The trade off is a reduced detection limit when the Sun is high. On average, the detection limit is $0.0066 \mu\text{W}/(\text{cm}^2 \text{nm})$ for $\text{SZA} < 65^\circ$, $0.0035 \mu\text{W}/(\text{cm}^2 \text{nm})$ for $65^\circ < \text{SZA} < 75^\circ$, and $0.0022 \mu\text{W}/(\text{cm}^2 \text{nm})$ for $\text{SZA} > 75^\circ$.

[38] The detection limit of the UV9, does not depend on SZA and varies between 0.0001 and $0.001 \mu\text{W}/(\text{cm}^2 \text{nm})$. The average value is $0.00033 \mu\text{W}/(\text{cm}^2 \text{nm})$. This is about one order of magnitude below the detection limit of the SUV-100.

[39] All spectra were also scrutinized for spikes, and other spectral anomalies using the V2 routines. Four spectra of the UV9 were found to be distorted, likely due to shading of the collector by personnel. SUV-100 spectra were free of conspicuous features.

7. Discussion

[40] The standard deviation of wavelength shifts of the SUV-100 spectroradiometer was 0.025 nm (Figure 3a). This value is about a factor of 1.8 larger than the standard deviation for January to March 2006. From 16 September 2006 onward, the wavelength mapping of the system's monochromator started to oscillate with a periodicity of about one month and this led to the increased wavelength uncertainty (NSF Polar Programs UV Spectroradiometer Network 2006–2007 Operations Report Volume 16.0, in preparation, available at www.biospherical.com/NSF). A similar oscillation has not been observed with any of the SUV-100 instruments before. The root cause of the problem is still unknown, but inspection of the monochromator in January 2007 pointed to excess friction in one of the monochromator's bearings. These variations can in theory

be corrected by applying a large number of correction functions, but this approach is impractical for operational data processing. Six correction functions were applied for the period of the campaign when final SUV-100 data were prepared. This number decreased the wavelength uncertainty from initially $\pm 0.05 \text{ nm}$ ($\pm 1\sigma$) to $\pm 0.025 \text{ nm}$. A wavelength uncertainty of $\pm 0.025 \text{ nm}$ translates into an uncertainty in measuring erythemal irradiance of about $\pm 0.5\%$ [Bernhard and Seckmeyer, 1999].

[41] Analysis of UV9 spectra revealed a systematic wavelength shift of 0.04 nm (Figure 3b), which translates into an overestimate of erythemal irradiance of about 0.5%. This shift was not present in archived NIWA data prior to 2004, but affects NIWA data that have been archived for the periods between January 2004 and December 2005, when a different solar reference spectrum was in use. As a result of this study, NIWA data from all sites will be reprocessed and resubmitted to NDACC.

[42] Results of the intercomparison have shown that measurements of the SUV-100 were on average 5–7% lower than UV9 data. This deviation is within the expected uncertainty of high quality spectroradiometers [Bernhard and Seckmeyer, 1999; Bais et al., 2001]. Possible reasons for this difference are discussed below and summarized in Table 3.

[43] The calibration scale for the SUV-100 refers to the source-based scale NIST scale from 1990 (NIST1990) [Walker et al., 1987]. UV9 data refer to the newer detector-based NIST scale from 2002 [Yoon et al., 2002]. Irradiance values assigned to calibration standards using the new scale are 1.1–1.5% larger than values based on the NIST1990 scale. The difference in the primary irradiance scale explains about 1.3% of the difference between SUV-100 and UV9 measurements.

[44] The UV9 is equipped with a dome-shaped diffuser of 4.5 mm height. By adapting calculations performed for similar diffusers [Bernhard and Seckmeyer, 1997; Hovila et al., 2005], we estimated that the reference plane for irradiance calibrations could be about 2 mm behind the diffuser's top. Recent experimental evidence conflicts with theoretical calculations, indicating that the offset for shaped diffusers may exceed the height of the diffuser [Manninen et al., 2006; Gröbner and Blumthaler, 2007]. Preliminary tests with the UV9 diffuser have indicated that its reference plane could be as much as 5 mm behind the diffuser's top. The calibrations of solar data of the UV9 were performed with standard lamps mounted at 500 mm distance measured from

Table 3. Breakdown of Differences SUV-100 - UV9

Component	Difference ^a
Irradiance scale NSF–NIWA	$1.3 \pm 0.3\%$
Diffuser geometry UV9	$1.4 \pm 0.6\%$
Drift of SUV-100 calibration standards	$1.0 \pm 1.0\%$
Diffuser temperature dependence UV9	$0 \pm 1.4\%$
PMT high-voltage dependence SUV-100 ^b	$1.5 \pm 1.0\%$
Sum ^c	$5.2 \pm 2.1\%$

^aDifferences are given as a range, representing maximum explainable deviations. Systematic parts of all components go in the same direction and increase the difference between SUV-100 and UV9.

^bDifference is largest at small SZA.

^cThe range of $\pm 2.1\%$ was calculated by the root of sum of squares of the individual components.

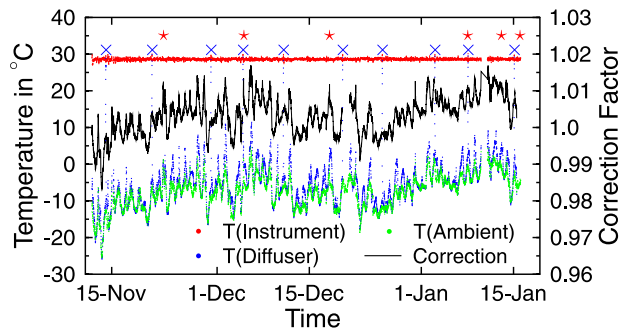


Figure 9. Time series of temperatures (instrument, diffuser and ambient air) logged by UV9. The black line shows the temperature correction factor that was applied to UV9 data. Crosses (stars) indicate times when UV9 (SUV-100) calibrations were performed.

the top of the diffuser. Theoretical and experimental evidence suggests that the diffuser may have been between 2 and 5 mm too far away from the lamp during calibrations. This would lead to an overestimate of solar measurements by 0.8–2.0%.

[45] The diffuser of the SUV-100 diffuser is effectively a flat membrane of PTFE with a thickness of 0.5 mm. The distance is measured from its front surface. The uncertainty in solar irradiance due to the diffuser thickness and shape is therefore less than 0.2%.

[46] The on-site calibrations standard of the SUV-100 spectroradiometer consist of three 200-W tungsten halogen lamps with calibrations provided by Optronic Laboratories and BSI (NSF Polar Programs UV Spectroradiometer Network 2006–2007 Operations Report Volume 16.0, in preparation, available at www.biospherical.com/NSF). Two of the three lamps were unstable at the 2–3% level during 2006. This was determined by a filtered, temperature-stabilized photodiode that is internal to the SUV-100. The third lamp was stable. The three lamps were also compared with traveling standard lamps in January 2006 and January 2007. In May 2007, these traveling standards were in turn compared with two 200-Watt long-term standard lamps maintained at BSI, as well as four 1000-W FEL lamps with calibrations from NOAA’s Central UV Calibration Facility (CUCF). Reanalysis of all available calibration information led to the conclusion that the calibration applied to SUV-100 solar data of the campaign was low by $1.0 \pm 1.0\%$.

[47] The transmission of the UV9’s Polytetrafluoroethylene (PTFE) diffuser changes with temperature [McKenzie *et al.*, 2005]. At 10°C (0°C) it is about 2.2% (1.5%) lower than at 20°C. Ylianttila and Schreder [2005] have reported a similar temperature dependence for Schreder J1002 PTFE diffusers. Their work also included a measurement at -5°C , indicating that diffuser transmissions at -5°C and 20°C are similar. Campaign data of the UV9 were corrected upwards by up to 2%, depending on the logged air temperature. Although the diffuser temperature was also recorded, it sometimes exceeded the air temperature by more than 5°C , which is an unrealistically large difference (Figure 9) and may be caused by absorption of radiation by the sensor’s black coating. On the basis of previous studies with an IR thermometer at Lauder, it was found that for small solar zenith angles and with clear skies, these dif-

fusers can only be up to 2°C warmer than ambient air temperature. A simple algorithm was used to predict the diffuser temperature as a function of air temperature, UV transmission, and solar zenith angle. For conditions during this campaign, the deduced diffuser temperature closely matches the air temperature, with a positive bias of up to 1°C around noon. Calibrations were performed at an instrument temperature of about 29°C (Figure 9). Corrections for the temperature dependence are typically in the range 0 to 2% (Figure 9). The uncertainty of the correction is about $\pm 1\%$ ($\pm 2\sigma$) and mostly due to the fact that the temperature coefficient has not been measured at temperatures below -5°C .

[48] The temperature coefficient of the SUV-100 diffuser is currently unknown. Since it is also made from PTFE, its temperature dependence may resemble that of the UV9, but the absolute value may be different due to its substantially smaller thickness. No temperature corrections were applied to SUV-100 data because both solar measurements and calibrations were carried out at ambient temperature. Variations in air temperatures between the biweekly calibrations result in an uncertainty of $\pm 1\%$. This value was estimated based on typical variations in temperature between calibrations (Figure 9) and the temperature coefficient of PTFE reported by McKenzie *et al.* [2005] and Ylianttila and Schreder [2005].

[49] The dependence of SUV-100 measurements on the high-voltage applied to the PMT discussed earlier can explain $1.5 \pm 1.0\%$ of the difference of SUV-100 and UV9 measurements. The reason of this nonlinearity is still not understood.

[50] The five factors listed above can explain $5.2 \pm 2.1\%$ of the difference between the two instruments. This number agrees well with the difference that was actually observed.

[51] Figure 4a shows statistics on the ratio of measured and modeled SUV-100 clear-sky spectra for the period of the campaign. Similar ratio-spectra have been presented by Bernhard *et al.* [2006b] for the years 1990–2004 for evaluating the consistency of SUV-100 measurements over the history of instrument operation at Arrival Heights. By comparing ratio-spectra from 2006 with this earlier analysis we are trying in the following to assess whether SUV-100 measurements from the intercomparison period are representative for measurements of the last 16 years. For this analysis, ratios at several wavelengths were extracted from the

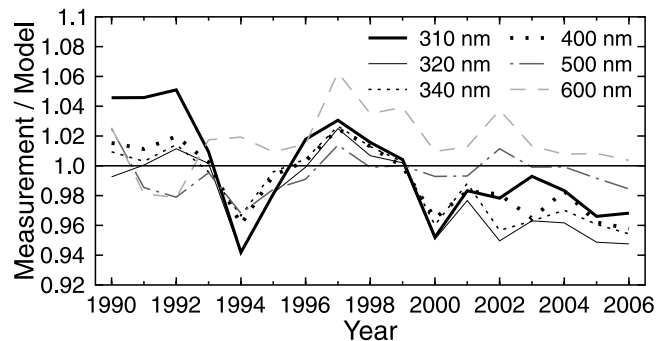


Figure 10. Ratio of SUV-100 measurements and model calculations of the years 1990–2006. The data set is based on median ratios for December.

previously calculated median-ratio-spectra for December and are shown in Figure 10. Ratios at all wavelengths range from 0.94 to 1.06. For wavelengths in the UV-A, values from the years 1990–1999 tend to be larger by about 3.5% than values from the years 2000–2006. This step-change is likely caused by a change of the instrument’s cosine error in February 2000, resulting from a modification of the irradiance collector [Bernhard *et al.*, 2006b]. Data indicate that the cosine error correction that is part of V2 processing has not completely removed the effect of collector change. Ratios for the intercomparison period are at the low end of the range: in the UV-A, ratios for December 2006 were on average 1.6% smaller than ratios of the years 2000–2005 and 5% smaller than ratios of the years 1990–1999. These differences should be considered when estimating trends in UV.

[52] Some of the variation shown in Figure 10 may have been caused by the model. For example, effective albedo used for modeling was calculated from the measured spectra, and potential errors in determining albedo may have changed over time. This shows that model calculations have limitations for quality control. However, in the absence of other supporting data, models present the only viable tool for assessing the consistency of measurements over time.

[53] A key objective of the campaign was to determine whether SUV-100 data from Arrival Heights and other sites of the UVSIMN adhere to the standards established by NDACC [McKenzie *et al.*, 1997]. UV data submitted to the NDACC databases have to meet certain specifications and must have successfully participated in an intercomparison with an already certified instrument. Our analysis shows that SUV-100 instruments meet the NDACC specifications for UV spectroradiometer with the following three exceptions: (1) NDACC calls for cosine errors of smaller than $\pm 5\%$ for zenith angles smaller than 60° ; the cosine error of the SUV-100 at 60° is -8.5% (Table 1). The ratio of SUV-100 to UV9 showed very little dependence on SZA, both for clear-sky and cloudy conditions (Figure 5). This demonstrates that V2 processing corrects the effect of the cosine error with adequate accuracy for the conditions observed during the campaign, which are typical for high-latitude NSF network sites (e.g., no cumulus clouds). The increased cosine error of the system is considered acceptable since NDACC specifications refer to the quality of submitted data rather than the characteristics of instrumentation. (2) NDACC calls for a wavelength alignment precision of $\leq \pm 0.03$ nm and accuracy of $\leq \pm 0.05$ nm ($\pm 2\sigma$). The wavelength variability of SUV-100 data is on average ± 0.05 nm at the 2σ -level (Figure 3a). This has less impact in polar regions where long-term changes in UV radiation are expected to be larger than at midlatitudes. Long-term drifts of the wavelength scale are effectively eliminated by the V2 wavelength correction. (3) NDACC calls for a detection threshold of smaller than $1 \mu\text{Wm}^{-2} \text{nm}^{-1}$ for a signal-to-noise ratio of 1. This low value was chosen for detecting small changes in UV-B irradiance in response to changes in total ozone. The detection threshold of the SUV-100 calculated with this definition is $7 \mu\text{Wm}^{-2} \text{nm}^{-1}$. Although SUV-100 spectroradiometers do not meet all specifications established by the NDACC, the intercomparison has demonstrated that data of the UVSIMN are of acceptable quality and inclusion in the NDACC database should therefore be

justified as long as data limitations are documented in complementing metafiles.

8. Conclusions

[54] Measurements of global spectral irradiance from a SUV-100 spectroradiometer permanently installed at Arrival Heights were compared with those of NIWA’s UV9 instrument. Measurements by the SUV-100 were on average lower by 5–7% than data of the UV9. This level of discrepancy compares well with results from earlier inter-comparisons of NSF and NIWA instruments [Seckmeyer *et al.*, 1995; Wuttke *et al.*, 2006a], as well as outcomes of other inter-comparisons of state-of-the-art UV spectroradiometers [Bais *et al.*, 2001]. The difference of measurements of the two instruments was very constant over time and showed little dependence on wavelength, SZA, and sky condition. This confirms that the V2 method is able to correct the comparatively large cosine error of the SUV-100 instrument with little uncertainty. The discrepancy of the two data sets has been quantitatively explained by different irradiance scales used by NSF and NIWA (difference of $1.3 \pm 0.3\%$); uncertainties in determining the reference plane of the UV9 diffuser ($1.4 \pm 0.6\%$); drifts of SUV-100 calibration standards ($1.0 \pm 1.0\%$); uncertainty due to the temperature-dependent transmission of diffusers ($0 \pm 1.4\%$); and non-linearity of the SUV-100 ($1.5 \pm 1.0\%$). The analysis also revealed a systematic wavelength offset of 0.04 nm in the UV9 data, which will be corrected as a result of this work. Many of the factors affecting data quality would have been difficult to detect without a second instrument. This highlights the value of the intercomparison.

[55] Measurements were also compared with results of a radiative transfer model. UV9 measurements are in better agreement with the calculations, but uncertainties in effective albedo limit the ability of the model in determining the radiometric accuracy of measurements. Wavelength shifts in measured spectra calculated with the V2 and SHICrvm methods were consistent to the 0.005 nm level. Both methods uncovered a wavelength bias in the UV9 data set, which was subsequently reprocessed. The bias of the revised data set was smaller than 0.005 nm on average, and stable to within ± 0.0025 nm over the course of the campaign. The wavelength registration of the SUV-100 fluctuated on the ± 0.025 nm level, partly due to excess friction affecting its monochromator during the period of the inter-comparison. The SUV-100 does not meet all specifications for UV spectroradiometry established by the NDACC, specifically those for the cosine error, short-term wavelength stability, and detection limit. However, results of the campaign have shown that the V2 method can accurately correct the shortcomings of the instrument. It is therefore justified to contribute SUV-100 data to the NDACC databases. Results of the comparison will be useful when data from other sites of the NSF UVSIMN and NIWA networks are combined for investigating geographical differences in ultraviolet irradiance. Such a study is planned for the near future.

[56] **Acknowledgments.** Measurements of the SUV-100 spectroradiometer at Arrival Heights were supported by the National Science Foundation’s Office of Polar Programs via a subcontract to Biospherical Instruments Inc. from Raytheon Polar Services Company (RPSC). We

particularly wish to express our gratitude to Steve Dobbs and Jason Bryenton from RPSC, who operated the SUV-100 instrument during this campaign. Further thanks go to Vi Quang from BSI for assisting in data processing. We thank Harry Slaper from the National Institute for Public Health and the Environment of The Netherlands for making the SHICrvm program available. Ozone sonde measurements used for modeling were provided by Terry Deshler from the University of Wyoming. OMI overpass data were retrieved from the Aura Validation Data Center at http://avdc.gsfc.nasa.gov/phpgdv2/avdc_tablefile.php?id=28. Atmospheric pressure data were made available by Matthew Lazzara, University of Wisconsin-Madison, and downloaded from <ftp://amrc.ssec.wisc.edu/pub/mcmurdo/arrivalheights/>. We also acknowledge the support of Antarctica NZ for transporting and staging the NIWA instrument, and the UV9 operators Penny Clendon and Nathan Cross. We thank Gunther Seckmeyer from the University of Hannover, Germany, for valuable comments to the manuscript and fruitful discussions regarding the NDACC requirements.

References

- Badosa, J., R. L. McKenzie, P. V. Johnston, M. Kotkamp, M. O'Neill, and D. J. Anderson (2007), Towards closure between measured and modelled UV under clear skies at four diverse sites, *Atmos. Chem. Phys.*, *7*, 2817–2837. Available at www.atmos-chem-phys.net/7/2817/2007/
- Bais, A. F., et al. (2001), SUSPEN intercomparison of ultraviolet spectroradiometers, *J. Geophys. Res.*, *106*(D12), 12,509–12,526.
- Balis, D., M. Kroon, M. E. Koukoulis, E. J. Brinkma, G. Labow, J. P. Veefkind, and R. D. McPeters (2007), Validation of Ozone Monitoring Instrument total ozone column measurements using Brewer and Dobson spectrophotometer ground-based observations, *J. Geophys. Res.*, *112*, D24S46, doi:10.1029/2007JD008796.
- Bernhard, G., and G. Seckmeyer (1997), New entrance optics for solar spectral UV measurements, *Photochem. Photobiol.*, *65*(6), 923–930.
- Bernhard, G., and G. Seckmeyer (1999), Uncertainty of measurements of spectral solar UV irradiance, *J. Geophys. Res.*, *104*(D12), 14,321–14,345.
- Bernhard, G., C. R. Booth, and R. D. McPeters (2003), Calculation of total column ozone from global UV spectra at high latitudes, *J. Geophys. Res.*, *108*(D17), 4532, doi:10.1029/2003JD003450.
- Bernhard, G., C. R. Booth, and J. C. Ebrahimian (2004), Version 2 data of the National Science Foundation's Ultraviolet Radiation Monitoring Network: South Pole, *J. Geophys. Res.*, *109*, D21207, doi:10.1029/2004JD004937.
- Bernhard, G., C. R. Booth, J. C. Ebrahimian, and V. V. Quang (2006a), NSF Polar Programs UV Spectroradiometer Network 2004–2005 Operations Report Volume 14.0, Biospherical Instruments Inc., San Diego. Available at www.biospherical.com/NSF
- Bernhard, G., C. R. Booth, J. C. Ebrahimian, and S. E. Nichol (2006b), UV climatology at McMurdo Station, Antarctica, based on Version 2 data of the National Science Foundation's Ultraviolet Radiation Monitoring Network, *J. Geophys. Res.*, *111*, D11201, doi:10.1029/2005JD005857.
- Bernhard, G., C. R. Booth, J. C. Ebrahimian, R. Stone, and E. G. Dutton (2007), Ultraviolet and visible radiation at Barrow, Alaska: Climatology and influencing factors on the basis of version 2 National Science Foundation network data, *J. Geophys. Res.*, *112*, D09101, doi:10.1029/2006JD007865.
- Booth, C. R., and S. Madronich (1994), Radiation amplification factors: Improved formulation accounts for large increases in ultraviolet radiation associated with Antarctic ozone depletion, edited by C. S. Weiler and P. A. Penhale, *Antarc. Res. Ser.*, *62*, 39–42, AGU, Washington, DC.
- Booth, C. R., T. B. Lucas, J. H. Morrow, C. S. Weiler, and P. A. Penhale (1994), The United States National Science Foundation's polar network for Monitoring Ultraviolet Radiation, edited by C. S. Weiler and P. A. Penhale, *Antarc. Res. Ser.*, *62*, 17–37, AGU, Washington, DC.
- Bouillon, R., J. Eisman, M. Garabedian, M. Holick, J. Kleinschmidt, T. Suda, I. Terenetskaya, and A. Webb (2006), Action spectrum for the production of previtamin D3 in human skin, CIE publication 174:2006, Commission Internationale de l'Éclairage (CIE), Vienna, Austria.
- Caldwell, M. M. (1971), Solar UV irradiation and the growth and development of higher plants, in *Photophysiology*, edited by A. C. Giese, vol. 6, Chapter 4, pp. 131–177, Academic Press, New York.
- Day, T. A., C. T. Ruhland, C. W. Grobe, and F. Xiong (1999), Growth and reproduction of Antarctic vascular plants in response to warming and UV radiation reductions in the field, *Oecologia*, *119*, 24–35.
- Early, A., et al. (1998), The 1995 North American interagency intercomparison of ultraviolet monitoring spectroradiometers, *J. Res. Natl. Inst. Stand. Technol.*, *103*(1), 15.
- Greenblatt, G. D., J. J. Orlando, J. B. Burkholder, and A. R. Ravishankara (1990), Absorption measurements of Oxygen between 330 and 1140 nm, *J. Geophys. Res.*, *95*(D11), 18,577–18,582.
- Gröbner, J., and M. Blumthaler (2007), Experimental determination of the reference plane of shaped diffusers by solar ultraviolet measurements, *Opt. Lett.*, *32*(1), 80–82.
- Gueymard, C. A. (2004), The sun's total and spectral irradiance for solar energy applications and solar radiation models, *Sol. Energy*, *76*(4), 423–453.
- Hovila, J., M. Mustonen, P. Kärhä, and E. Ikonen (2005), Determination of the diffuser reference plane for accurate illuminance responsivity calibrations, *Appl. Opt.*, *44*(28), 5894–5898.
- Kalliskota, S., J. Kaurola, P. Taalas, J. Herman, E. Celarier, and N. Krotkov (2000), Comparison of daily UV doses estimated from Nimbus 7/TOMS measurements and ground-based spectroradiometric data, *J. Geophys. Res.*, *105*(D4), 5059–5067.
- Kancler, E., C. Gautier, P. Ricchiazzi, S. Yang, and P. Pilewskie (2005), Spectral observations and modeling of the Arctic surface radiation environment, *J. Geophys. Res.*, *110*, D23203, doi:10.1029/2005JD005813.
- Kneizys, F. X., E. P. Shettle, W. O. Gallery, J. H. Chetwynd, L. W. Abreu, J. E. A. Selby, S. A. Clough, and R. W. Fenn (1983), Atmospheric transmittance/radiance: Computer code LOWTRAN 6, in *AFGL Environmental Research Papers*, Air Force Geophysics Laboratory, Report AFGL-TR-83-0187, Hanscom Air Force Base, MA.
- Kurucz, R. L., I. Furenlid, J. Brault, and L. Testerman (1984), Solar flux atlas from 296 to 1300 nm, National Solar Observatory Atlas No. 1, Harvard Univ. Press, Cambridge, Mass. Available at <ftp://ftp.noao.edu/fts/fluxat/>
- Lantz, K., et al. (2002), The 1997 North American interagency intercomparison of ultraviolet spectroradiometers including narrowband filter radiometers, *J. Res. Natl. Inst. Stand. Technol.*, *107*, 19–62.
- Lenoble, J., A. Kylling, and I. Smolskaia (2004), Impact of snow cover and topography on ultraviolet irradiance at the Alpine station of Briançon, *J. Geophys. Res.*, *109*, D16209, doi:10.1029/2004JD004523.
- Madronich, S., and S. Flocke (1998), The role of solar radiation in atmospheric chemistry, in *Handbook of Environmental Chemistry*, edited by P. Boule, pp. 1–26, Springer, Heidelberg.
- Manninen, P., J. Hovila, L. Seppälä, P. Kärhä, L. Ylianttila, and E. Ikonen (2006), Determination of distance offsets of diffusers for accurate radiometric measurements, *Metrologia*, *43*, S120–S124, doi:10.1088/0026-1394/43/2/S24.
- Mayer, B., and A. Kylling (2005), Technical note: The libRadtran software package for radiative transfer calculations – Description and examples of use, *Atmos. Chem. Phys.*, *5*, 1855–1877. Available at www.atmos-chem-phys.org/acp/5/1855/
- Mayer, B., A. Kylling, S. Madronich, and G. Seckmeyer (1998), Enhanced absorption of UV radiation due to multiple scattering in clouds: Experimental evidence and theoretical explanation, *J. Geophys. Res.*, *103*(D23), 31,241–31,254.
- McKenzie, R. L., P. V. Johnston, M. Kotkamp, A. Bittar, and J. D. Hamlin (1992), Solar ultraviolet spectroradiometry in New Zealand: Instrumentation and sample results from 1990, *Appl. Opt.*, *31*, 6501–6509.
- McKenzie, R. L., P. V. Johnston, and G. Seckmeyer (1997), UV spectroradiometry in the network for the detection of stratospheric change (NDSC), in *Solar Ultraviolet Radiation. Modelling, Measurements and Effects*, edited by C. S. Zerefos and A. F. Bais, pp. 279–287, Springer, Berlin.
- McKenzie, R., J. Badosa, M. Kotkamp, and P. Johnston (2005), Effects of the temperature dependence in PTFE diffusers on observed UV irradiances, *Geophys. Res. Lett.*, *32*, L06808, doi:10.1029/2004GL022268.
- McKinlay, A. F., and B. L. Diffey (Eds.) (1987), A reference action spectrum for ultraviolet induced erythema in human skin, in: *Commission Internationale de l'Éclairage (CIE), Research Note*, *6* (1), 17–22, Commission Internationale de l'Éclairage (CIE), Vienna, Austria.
- Nichol, S. E., G. Pfister, G. E. Bodeker, R. L. McKenzie, S. W. Wood, and G. Bernhard (2003), Moderation of cloud reduction of UV in the Antarctic due to high surface albedo, *J. Appl. Meteorol.*, *42*(8), 1174–1183.
- Seckmeyer, G., et al. (1995), Geographical differences in the UV measured by intercompared spectroradiometers, *Geophys. Res. Lett.*, *22*(14), 1889–1892.
- Seckmeyer, G., A. Bais, G. Bernhard, M. Blumthaler, C. R. Booth, P. Disterhoft, P. Eriksen, R. L. McKenzie, M. Miyauchi, and C. Roy (2001), Instruments to measure solar ultraviolet radiation. part I: Spectral instruments, World Meteorological Organisation, Global Atmospheric Watch Publication No. 125, WMO TD No. 1066, World Meteorological Organization, Geneva, Switzerland.
- Setlow, R. B. (1974), The wavelength in sunlight effective in producing skin cancer: A theoretical analysis, *Proc. Natl. Acad. Sci. U.S.A.*, *71*(9), 3363–3366.
- Slaper, H., and T. Koskela (1997), Methodology of intercomparing spectral sky measurements, in *The Nordic Intercomparison of Ultraviolet and Total Ozone Instruments at Izaña, October 1996, Final Report*, edited

- by B. Kjeldstad, B. Johnsen, and T. Koskela, Finnish Meteorol. Inst., Helsinki.
- Slaper, H., H. A. J. M. Reinen, M. Blumthaler, M. Huber, and F. Kuik (1995), Comparing ground-level spectrally resolved solar UV measurements using various instruments: A technique resolving effects of wavelength shift and slit width, *Geophys. Res. Lett.*, *22*(20), 2721–2724.
- Smith, R. C., et al. (1992), Ozone depletion: Ultraviolet radiation and phytoplankton biology in Antarctic waters, *Science*, *256*, 952–959.
- Stamnes, K., J. Slusser, and M. Bowen (1991), Derivation of total ozone abundance and cloud effects from spectral irradiance measurements, *Appl. Opt.*, *30*, 4418–4426.
- Tanskanen, A., et al. (2007), Validation of daily erythemal doses from Ozone Monitoring Instrument with ground-based UV measurement data, *J. Geophys. Res.*, *112*, D24S44, doi:10.1029/2007JD008830.
- Thompson, A., et al. (1997), The 1994 North American interagency inter-comparison of ultraviolet monitoring spectroradiometers, *J. Res. Natl. Inst. Stand. Technol.*, *102*(3), 279–322.
- van Hoosier, M. E. (1996), Solar ultraviolet spectral irradiance data with increased wavelength and irradiance accuracy, in *Ultraviolet Atmospheric and Space Remote Sensing: Methods and Instrumentation*, edited by R. E. Huffman and C. G. Stergis, *Proc. SPIE Int. Soc. Opt. Eng.*, *2831*, 57–64, SPIE, Bellingham, WA.
- Walker, J. H., R. D. Saunders, J. K. Jackson, and D. A. McSparron (1987), Spectral irradiance calibrations, NBS Spec. Publ. U. S., 250–20, Natl. Bureau of Standards, Washington, D. C.
- Wuttke, S., G. Seckmeyer, G. Bernhard, J. Ebrahimian, R. McKenzie, P. Johnston, and M. O’Neil (2006a), New spectroradiometers complying with the NDSC standards, *J. Atmos. Oceanic Technol.*, *23*(2), 241–251.
- Wuttke, S., G. Seckmeyer, and G. König-Langlo (2006b), Measurements of spectral snow albedo at Neumayer, Antarctica, *Ann. Geophys.*, *24*, 7–21.
- Ylianttila, L., and J. Schreder (2005), Temperature effects on PTFE diffusers, *J. Opt. Materials*, *27*, 1811–1814.
- Yoon, H. W., C. E. Gibson, and P. Y. Barnes (2002), Realization of the National Institute of Standards and Technology detector-based spectral irradiance scale, *Appl. Opt.*, *41*(28), 5879–5890.
- Zerefos, C., D. Balis, M. Tzortziou, A. Bais, K. Tourpali, C. Meleti, G. Bernhard, and J. Herman (2001), A note on the interannual variations of UV-B erythemal doses and solar irradiance from ground-based and satellite observations, *Ann. Geophys.*, *19*, 115–120.
-
- G. Bernhard, C. R. Booth, and J. C. Ebrahimian, Biospherical Instruments Inc., 5340 Riley Street, San Diego, CA 92110-2621, USA. (bernhard@biospherical.com)
- P. Johnston, M. Kotkamp, R. L. McKenzie, and S. Wood, National Institute of Water and Atmospheric Research (NIWA), Lauder, Private Bag 50061, Omakau 9352, Central Otago, New Zealand.
- S. E. Nichol, National Institute of Water and Atmospheric Research (NIWA), Kilbirnie, Private Bag 14901, Wellington 6241, New Zealand.